



Synthesis of 2-amino-3-cyano-4*H*-pyran derivatives using GO-Fc@Fe₃O₄ nanohybrid as a novel recyclable heterogeneous nanocatalyst and preparation of tacrine-naphthopyran hybrids as AChE inhibitors

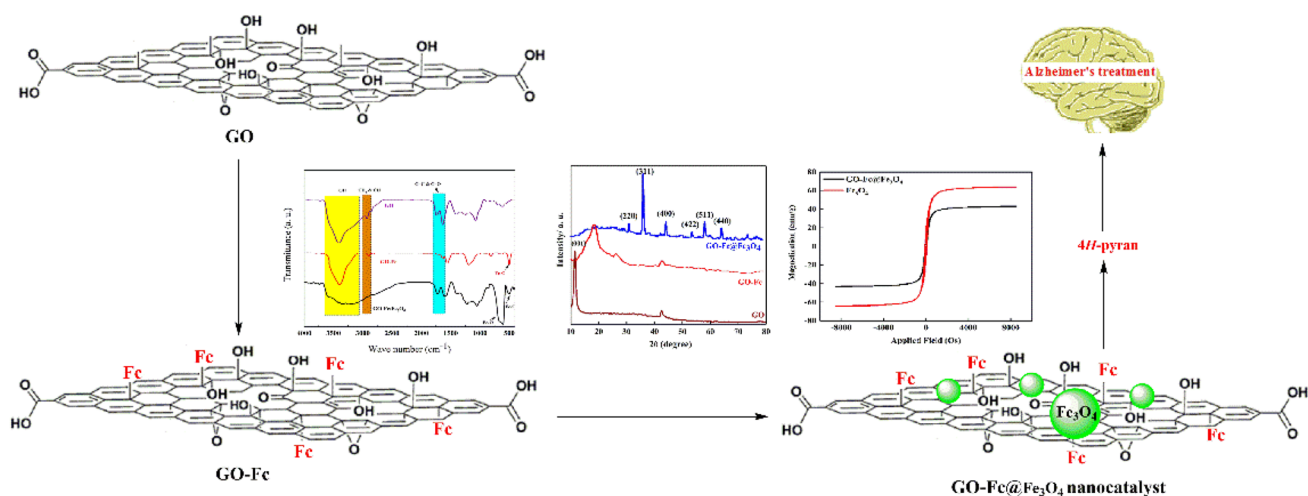
Sakineh Mozaffarnia^{1,2} · Reza Teimuri-Mofrad¹ · Mohammad-Reza Rashidi²

Received: 26 July 2020 / Accepted: 27 November 2020 / Published online: 3 January 2021
© Iranian Chemical Society 2021

Abstract

GO-Fc@Fe₃O₄ nanohybrid as a powerful and reusable nanocatalyst was synthesized. The graphene oxide (GO) sheets with meta-chloroperoxybenzoic acid (mCPBA) were treatment, afterward were chemically modified with 4-Fc derivative through the ring-opening reaction between GO nanosheets and 4-ferrocenylbutylamine. Then, the final nanocatalyst was obtained by synthesizing of Fe₃O₄ nanoparticles onto the modified GO surface. The structure and morphology of GO-Fc@Fe₃O₄ nanohybrid were characterized using different analysis, such as FT-IR, XRD, FE-SEM, EDX, and VSM techniques. Then, 2-amino-3-cyano-4*H*-pyran derivatives (**4a–l**) as a synthetic precursor were synthesized via multi-component reaction in the presence of GO-Fc@Fe₃O₄ nanohybrid as a novel heterogeneous nanocatalyst. Finally, according to the importance of finding a solution to treat Alzheimer's disease, 14-aryl-10,11,12,14-tetrahydro-9*H*-benzo[5,6]chromeno[2,3-*b*]-quinolin-13-amines (**5a–l**) as new tacrine-naphthopyran hybrid analogs were designed and prepared as acetylcholinesterase inhibitors. These compounds were synthesized via Friedländer reaction of 2-amino-3-cyano-4*H*-pyran derivatives (**4a–l**) with cyclohexanone. HACHe inhibition assay was carried out in vitro on the synthesized compounds **5a–l**. Among them, compound **5f** exhibited potent hAChE inhibitors with IC₅₀ values of 0.16 μM. Also, the molecular docking and kinetic studies performed for a better understanding of compound **5f** as a representative compound.

Graphic abstract



Keywords GO-Fc@Fe₃O₄ nanohybrid · Multi-component reaction · Solvent-free · Tacrine hybrid · Molecular modeling

✉ Reza Teimuri-Mofrad
teymouri@tabrizu.ac.ir

Extended author information available on the last page of the article

Abbreviations

AD	Alzheimer's disease
ACh	Acetylcholine
AChE	Acetylcholinesterase
BuChE	Butyrylcholinesterase
ChEI	Cholinesterase inhibitor
PAS	Peripheral anionic site
CAS	Catalytic active site
GO	Graphene oxide
mCPBA	<i>meta</i> -Chloroperoxybenzoic acid

Introduction

Alzheimer's disease (AD) is an irreversible and multifactorial neurodegenerative illness and the main cause of dementia in elderly people [1–3]. AD begins with memory loss in the early stages and gradually develops in the advanced stages of cognitive impairment, causing severe behavioral abnormalities and eventually leading to death [4–7]. Due to the increased life expectancy and the number of elderly people, AD has become an important public health issue [8, 9]. AD pathophysiology is not yet fully clear, but factors other than age and heredity are involved as a shortage of acetylcholine (ACh), beta-amyloid (A β) aggregates, τ -protein aggregation, oxidative stress, mitochondrial dysfunction, and neuroinflammation [10–14]. There is not a definitive cure for AD, but one effective therapy for AD is increasing ACh levels in the brain by the inhibition of acetylcholinesterase (AChE) [15–17]. Acetylcholinesterase inhibitors including donepezil, rivastigmine, tacrine, and galantamine were used to treat AD [18, 19]. Tacrine was the first developed reversible cholinesterase inhibitor (ChEI) that was approved by the US FDA for the therapy for AD in 1993. Nevertheless, due to hepatotoxicity and peripheral side effects, it was approximately removed from the market. Tacrine is synthesized by Friedländer-type cyclocondensation of *o*-aminobenzonitrile with cyclohexanone [20–25]. Currently, research is ongoing on tacrine to design and synthesis new tacrine-based drugs via Friedländer reaction for modification on the structure of tacrine by the exchange of benzene rings in tacrine with other synthetic compounds [7, 26, 27]. The Friedländer reaction has been known for more than a century and is a well-known and simplest method for synthesis of different nitrogen-containing heterocyclic compounds such as quinoline derivatives, tacrine analogs, acridines, pyridines, campothecins, and phenanthrolines [28–30].

Pyran is one of the main core units in several natural and synthetic products. Organic molecules with 4*H*-pyran ring have biological and potential medical such as anti-allergic, antitumor, antibacterial, anti-HIV, antifungal, anti-coagulant, anti-cancer, anti-inflammatory, and neurodegenerative disorders [31–36]. Naphthopyran derivatives show

a variety of biological activities as anti-hypertensive, anti-coagulant, anti-allergic, anticancer, and antiviral activities. Also, organic photochromic naphthopyrans have an industrial applications of technology and used in manufacturing in plastic photochromic lenses (T-type photochromism). Due to the medicinal properties of pyran derivatives, it is important to use appropriate synthesis methods. One of the methods used is synthesis via a multi-component reaction in the presence of a suitable catalyst [37–45]. On the other hand, multi-component, solvent-free, and reusable heterogeneously catalyzed reactions are factors for the principles of green chemistry. Multi-component reactions are very strong and effective bond-forming tools in organic chemistry with high atom efficiency, time and energy saving, friendly environment, and rapid and simple efficiency. Also, the catalyst plays a significant role in selectivity and determining yield. So, the creation of a reusable, mild, inexpensive catalyst for multi-component reactions has attracted interest. The catalysts have been used for multi-component reactions, including ZnAl₂O₄-Bi₂O₃, SiO₂ NPs, Fe₃O₄@SiO₂@imidazol-bisFc[HCO₃], Fe₃O₄@SiO₂-BenzIm-Fc[Cl]/NiCl₂, SiO₂@Imid-Cl@Fc, and silica-bonded aminoethylpiperazine [33, 46–51]. The use of an efficient and stable heterogeneous catalyst as reusable and environmentally friendly substances has a very important role in organic synthesis. Also, the immobilization of catalyst on the solid supports have advantages such as non-toxicity, low solubility, increased reactions selectivity, and easy handling and led to the widespread use of these catalysts. Catalysts immobilized on the nanoparticle supports are more attractive, because of their higher selectivity and activity. Magnetite (Fe₃O₄) nanoparticle with unique properties such as high surface area, low toxicity, superparamagnetism, thermal stability, low cost, easy separation from the reaction mixture and recyclability used in the design and synthesis of reusable heterogeneous catalysts [49, 52–56].

Ferrocene derivatives have become very important for their applications such as redox electrochemistry, catalysis, biology, materials science, and nonlinear optical materials. Also, characteristics such as thermal stability, low cost, high tolerance to moisture, and oxygen make these materials attractive [57, 58]. Graphene oxide (GO) is one of the most important derivatives and the oxidized forms of graphene. GO has different oxygen groups such as hydroxyl, carboxyl, epoxide and carbonyl on its surface. Also, it has properties such as good chemical and mechanical stability, high conductivity and a special surface, and various applications such as energy storage materials, polymer nanocomposites and electrocatalysis [59–61].

In this work, GO-Fc@Fe₃O₄ nanohybrid as a new, powerful, and reusable nanocatalyst was synthesized. The modified GO nanosheets provide a large available surface area with several acidic and basic sites including carboxylic acid, hydroxyl, Fc rings on the GO-Fc surface. This nanocatalyst

was used to synthesize of 2-amino-3-cyano-4*H*-pyran derivatives (**4a–l**) under solvent-free conditions (Fig. 1). The desired products were obtained with good yield and in a short time. Compounds **4a–l** were used as precursors in the Friedländer reaction with cyclohexanone and under the usual experimental conditions were obtained 14-aryl-10,11,12,14-tetrahydro-9*H*-benzo[5,6]chromeno[2,3-*b*]-quinolin-13-amines derivatives (**5a–l**) as new tacrine analogs for inhibition of acetylcholinesterase enzyme (Fig. 1). The amount of hAChE and hBuChE enzymes inhibitory activity was investigated for these compounds and the results showed that this series of compounds have good inhibition only against hAChE enzyme.

Experimental

Materials and instruments

Commercially available compounds were bought from Merck and Sigma-Aldrich. Commercial compounds contain: graphene oxide (GO), sodium nitrate (NaNO₃) (CAS number: 7631-99-4), potassium permanganate (KMnO₄) (CAS number: 7722-64-7), sulfuric acid (H₂SO₄) (CAS number: 7664-93-9), hydrogen peroxide solution (H₂O₂) (CAS number: 7722-84-1), meta-chloroperoxybenzoic acid (mCPBA) (CAS number: 937-14-4), glacial acetic acid (CAS number: 64-19-7), iron(II) chloride tetrahydrate (FeCl₂·4H₂O) (CAS number: 13478-10-9), iron(III) chloride hexahydrate (FeCl₃·6H₂O) (CAS number: 10025-77-1), 2-naphthol (CAS number: 135-19-3), 6-bromo-2-naphthol (CAS number: 15231-91-1), malononitrile (CAS number: 109-77-3), benzaldehyde (CAS number: 100-52-7), 4-nitrobenzaldehyde (CAS number: 555-16-8), 4-methylbenzaldehyde (CAS number: 104-87-0), 4-isopropylbenzaldehyde (CAS number: 122-03-2), 4-chlorobenzaldehyde (CAS number: 104-88-1), 4-bromobenzaldehyde (CAS number: 1122-91-4), 2-chlorobenzaldehyde (CAS number: 89-98-5), 3-bromobenzaldehyde (CAS number: 3132-99-8), 4-fluorobenzaldehyde (CAS number: 459-57-4), thiophene-2-carbaldehyde (CAS number: 98-03-3), cyclohexanone (CAS number: 108-94-1), Aluminum chloride (AlCl₃) (CAS number: 7446-70-0), 1,2-dichloroethane (CAS number: 107-06-2). The reaction

progress was controlled by TLC and detected by UV light (254 nm). ¹H NMR and ¹³C NMR spectra were registered on Bruker Spectrospin Avance 400 and 100 MHz spectrometers in DMSO-*d*₆ solvent, respectively. All chemical shifts were reported as δ (ppm), and coupling constants (*J*) were given in Hz. The Bruker Tensor 27 tool was used to record the FT-IR spectra of the synthesized compound on the KBr pellets and expressed in cm⁻¹. Using an electric apparatus MEL-TEMP model 1202 was measured the melting point. Elementar Vario EL III tool was used for Elemental analysis (C, H, N). FESEM (TESCAN MIRA3), EDX spectroscopy (TESCAN MIRA3), and XRD analysis (PANalytica X pertPRO (Germany) instrument with Cu-Kα radiation (0.15406 nm) at accelerating voltage of 45 kV) were used to study the morphology and structure of the nanoparticles. Magnetization measurement was performed with a model 155 alternative gradient force magnetometer at room temperature.

Preparation of GO

Hummer's method was used to prepare GO nanosheets by oxidizing graphite flakes [62]. In brief, a round bottom flask was charged with graphite flake (2.5 g) and NaNO₃ (1.25 g). The flask was then immersed in an ice bath and 65 ml of concentrated H₂SO₄ was added to a flask and stirred for 1 h. Then, finely ground KMnO₄ was added in small portions into the above mixture under vigorous stirring at 0 °C. Vigorous stirring was continued for a further 72 h at 25 °C. After adding 175 ml of distilled water, 100 ml of HCl (10%) and 30 ml of H₂O₂ (30%) were slowly added to the above mixture and stirred for 2 h. After that, the mixture was centrifuged and washed with a large amount of deionized water to give GO powders.

Preparation of over-oxidized GO (GO-Epo)

An amount of 150 mg of mCPBA was added to a suspension of GO in DI water (25 ml, 3 mg/ml) and stirred at ambient temperature for 24 h. After this time, the reaction mixture was washed with dichloromethane to remove all the unreacted mCPBA. Then, the aqueous phase was centrifuged to give the over-oxidized GO nanosheets (GO-Epo) [63].

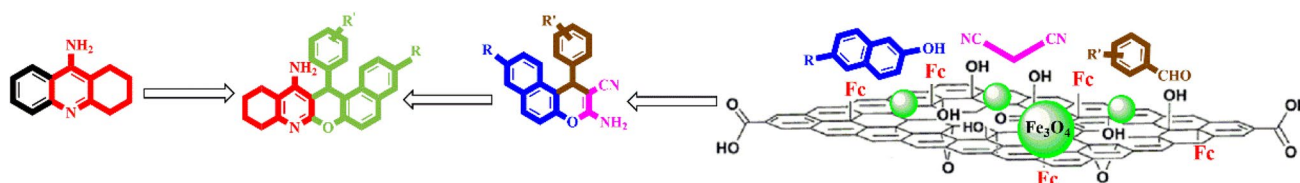


Fig. 1 Design and synthesis of 2-amino-3-cyano-4*H*-pyran (**4a–l**) and 14-aryl-10,11,12,14-tetrahydro-9*H*-benzo[5,6]chromeno[2,3-*b*]-quinolin-13-amines (**5a–l**) derivatives

Functionalization of GO-Epo with 4-ferrocenylbutylamine (GO-Fc)

An amount of 0.3 g of 4-ferrocenylbutylamine [64] was dissolved in 35 ml of ethanol and the resulted solution was then added to a suspension of GO-Epo in water (0.1 g in 30 ml water). The resulting mixture was refluxed for 72 h [60]. At the end of the reaction, the mixture was centrifuged and washed with water and dichloromethane, respectively. After vacuum drying, the GO-Fc was obtained as a black powder.

Synthesis of GO-Fc@Fe₃O₄ nanohybrid

A round bottom two necked flask was charged with FeCl₃·6H₂O (1.76 g, 6.5 mmol) and FeCl₂·4H₂O (0.65 g, 3.25 mmol). A mixture of glacial acetic acid (1.5 ml) and water (50 ml) was added to the above mixture under vigorous stirring. The appropriate amount of GO-Fc suspension was then added to the above flask and the temperature was raised from 25 to 80 °C. After the temperature reached to 80 °C, 10 ml of ammonia was added into the flask and allowed to stir for an additional 15 min at 80 °C. Finally, GO-Fc@Fe₃O₄ nanohybrid was separated by an external magnetic field and was washed with distilled water and methanol, respectively [65].

General procedure for the preparation of 2-amino-3-cyano-4H-pyran derivatives (4a–l)

A reaction vial was charged with 2-naphthol (**1a**) or 6-bromo-2-naphthol (**1b**) (1 mmol), aromatic aldehyde (**2a–j**) (1 mmol), malononitrile (**3**) (1.2 mmol), and GO-Fc@Fe₃O₄ (10 mg) as magnetic nanocatalyst. The mixture was heated at 100 °C under solvent-free conditions. After completion of the reaction (monitored by TLC), an appropriate amount of ethanol was added and the mixture heated for 5 min. Then, the magnetic nanocatalyst was separated by applying an external magnet. The crude solid was collected by filtration and then recrystallized from ethanol to give the pure compound.

General procedure for the synthesis of 14-aryl-10,11,12,14-tetrahydro-9H-benzo[5,6]chromeno[2,3-b]-quinolin-13-amines derivatives (5a–l)

AlCl₃ (1.5 equiv) and dry 1,2-dichloroethane (10 ml) were mixed at ambient temperature under argon atmosphere for 30 min. Then, compounds **4a–l** (1 equiv) and cyclohexanone (1.5 equiv) were added to them and heated at reflux for 24 h. Then, using a rotary evaporator was evaporated the solvent and NaOH 10% was added to the residual sediment and stirred for 30 min. The resulted mixture was filtered

and washed with EtOH. The synthesized compounds were obtained as solids.

14-(Phenyl)-10,11,12,14-tetrahydro-9H-benzo[5,6]chromeno[2,3-b]-quinolin-13-amine (5a)

Yield 92%; white solid; m.p. > 250 °C (mp. > 260 °C [22]).

14-(4-Nitrophenyl)-10,11,12,14-tetrahydro-9H-benzo[5,6]chromeno[2,3-b]-quinolin-13-amine (5b)

Yield 73%; white solid; m.p. > 250 °C (mp. 258–260 °C [66]).

14-(4-Methylphenyl)-10,11,12,14-tetrahydro-9H-benzo[5,6]chromeno[2,3-b]-quinolin-13-amine (5c)

Yield 59%; white solid; m.p. 223–227 °C (mp. 224–226 °C [66]).

14-(4-Isopropylphenyl)-10,11,12,14-tetrahydro-9H-benzo[5,6]chromeno[2,3-b]-quinolin-13-amine (5d)

Yield 57%; white solid; m.p. 239–244 °C. FTIR (KBr) ν 3492, 3355, 2931, 1617, 1444, 1227 cm⁻¹; ¹H NMR: 1.04 (d, 3H, ³J=0.9 Hz, CH₃), 1.05 (d, 3H, ³J=0.9 Hz, CH₃), 1.71 (br, 4H, CH₂), 2.21–2.25 (m, 1H, CH₂), 2.38–2.42 (m, 1H, CH₂), 2.63–2.64 (m, 2H, CH₂), 2.65–2.70 (m, 1H, CH), 6.17 (s, 1H, CH), 6.70 (br, 2H, NH₂), 7.04 (d, 2H, ³J=8.2 Hz, Ar-H), 7.42–7.47 (m, 4H, Ar-H), 7.55–7.59 (m, 1H, Ar-H), 7.91 (d, 2H, ³J=9.1 Hz, Ar-H), 8.36 (d, 1H, ³J=8.5 Hz, Ar-H); ¹³C NMR: 21.5, 21.6, 22.7, 23.6, 29.8, 32.8, 34.0, 99.7, 112.5, 117.3, 118.0, 123.4, 124.7, 126.2, 126.9, 127.5, 128.5, 129.0, 130.5, 130.6, 141.4, 146.5, 147.8, 149.1, 153.0, 153.3; Anal. Calcd. for C₂₉H₂₈N₂O (420.55): C 82.82, H 6.71, N 6.66; Found: C 82.89, H 6.70, N 6.59%.

14-(4-Chlorophenyl)-10,11,12,14-tetrahydro-9H-benzo[5,6]chromeno[2,3-b]-quinolin-13-amine (5e)

Yield 65%; white solid; m.p. > 250 °C. FTIR (KBr) ν 3418, 3206, 2940, 1648, 1478, 1226 cm⁻¹; ¹H NMR: 1.69–1.72 (m, 4H, CH₂), 2.21–2.25 (m, 1H, CH₂), 2.40–2.45 (m, 1H, CH₂), 2.72–2.73 (m, 2H, CH₂), 6.53 (s, 1H, CH), 7.26 (d, 2H, ³J=8.5 Hz, Ar-H), 7.44 (t, 1H, ³J=7.8 Hz, Ar-H), 7.49 (d, 1H, ³J=8.9 Hz, Ar-H), 7.55 (t, 1H, ³J=7.8 Hz, Ar-H), 7.63 (d, 2H, ³J=8.4 Hz, Ar-H), 7.92–7.99 (m, 2H, Ar-H), 8.36 (d, 1H, ³J=8.5 Hz, Ar-H); ¹³C NMR: 22.1, 22.3, 23.0, 32.0, 34.4, 99.0, 112.3, 115.8, 116.5, 117.8, 119.3, 124.3, 126.1, 128.7, 129.3, 129.6, 129.9, 130.5, 131.6, 143.0, 148.0, 148.8, 151.2, 152.3, 154.8. Anal. Calcd. for

$C_{26}H_{21}ClN_2O$ (412.91): C 75.63, H 5.13, N 6.78; Found: C 75.52, H 5.09, N 6.74%.

14-(2-Chlorophenyl)-10,11,12,14-tetrahydro-9H-benzo[5,6]chromeno[2,3-b]-quinolin-13-amine (5f)

Yield 92%; white solid; m.p. > 250 °C. FTIR (KBr) ν 3466, 3332, 2926, 1625, 1445, 1228 cm^{-1} ; 1H NMR: 1.70 (s, 4H, CH_2), 2.20–2.24 (m, 1H, CH_2), 2.32–2.39 (m, 1H, CH_2), 2.53–2.58 (m, 2H, CH_2), 5.66–5.67 (br, 2H, NH_2), 6.16 (s, 1H, CH), 7.10–7.14 (m, 1H, Ar-H), 7.16–7.20 (m, 1H, Ar-H), 7.35 (dd, 1H, $^3J=7.8, 1.2$ Hz, Ar-H), 7.39–7.46 (m, 3H, Ar-H), 7.52–7.55 (m, 1H, Ar-H), 7.89–7.92 (m, 2H, Ar-H), 8.25 (d, 1H, $^3J=8.0$ Hz, Ar-H); ^{13}C NMR: 22.0, 22.2, 22.9, 31.9, 34.1, 98.2, 112.4, 116.0, 117.9, 122.7, 124.3, 126.9, 127.0, 128.5, 128.6, 129.4, 129.5, 130.2, 130.4, 130.8, 131.5, 141.6, 149.0, 151.3, 152.7, 154.5; Anal. Calcd. for $C_{26}H_{21}ClN_2O$ (412.91): C 75.63, H 5.13, N 6.78; Found: C 75.70, H, 5.15, N 6.81%.

14-(4-Bromophenyl)-10,11,12,14-tetrahydro-9H-benzo[5,6]chromeno[2,3-b]-quinolin-13-amine (5g)

Yield 81%; white solid; m.p. > 250 °C. FTIR (KBr) ν 3453, 3406, 2928, 1629, 1442, 1231 cm^{-1} ; 1H NMR: 1.70 (br, 4H, CH_2), 2.19–2.23 (m, 1H, CH_2), 2.37–2.42 (m, 1H, CH_2), 2.571–2.578 (m, 2H, CH_2), 6.05 (s, 2H, NH_2), 6.13 (s, 1H, CH), 7.35–7.46 (m, 6H, Ar-H), 7.55 (t, 1H, $^3J=7.2$ Hz, Ar-H), 7.87–7.90 (m, 2H, Ar-H), 8.29 (d, 1H, $^3J=8.5$ Hz, Ar-H); ^{13}C NMR: 22.1, 22.2, 23.0, 32.0, 34.5, 98.8, 112.3, 117.3, 117.8, 119.3, 123.0, 124.3, 126.8, 128.5, 128.9, 129.7, 130.2, 130.6, 131.0, 144.1, 148.8, 151.2, 152.3, 154.8; Anal. Calcd. for $C_{26}H_{21}BrN_2O$ (457.36): C 68.28, H 4.63, N 6.12; Found: C 68.22, H 4.61, N 6.15%.

3-Bromo-14-(3-bromophenyl)-10,11,12,14-tetrahydro-9H-benzo[5,6]chromeno[2,3-b]-quinolin-13-amine (5h)

Yield 78%; white solid; m.p. > 250 °C. FTIR (KBr) ν 3425, 3152, 2934, 1651, 1412, 1230 cm^{-1} ; 1H NMR: 1.73–1.74 (m, 4H, CH_2), 2.25 (br, 1H, CH_2), 2.40 (br, 1H, CH_2), 2.73 (br, 2H, CH_2), 6.39 (s, 1H, CH), 7.19 (t, 1H, $^3J=7.8$ Hz, Ar-H), 7.34 (dd, 1H, $^3J=7.1, 0.7$ Hz, Ar-H), 7.44 (d, 1H, $^3J=7.8$ Hz, Ar-H), 7.61 (d, 1H, $^3J=9.0$ Hz, Ar-H), 7.82 (dd, 2H, $^3J=7.0, 1.9$ Hz, Ar-H), 7.89 (s, 1H, Ar-H), 8.02 (d, 1H, $^3J=9.1$ Hz, Ar-H), 8.23 (d, 1H, $^3J=9.1$ Hz, Ar-H), 8.30 (d, 1H, $^3J=1.0$ Hz, Ar-H); ^{13}C NMR: 22.5, 22.7, 23.5, 32.4, 35.4, 99.3, 111.4, 113.5, 117.6, 121.8, 122.2, 124.3, 126.2, 128.4, 128.9, 130.2, 130.5, 130.9, 131.4, 131.9, 132.3, 147.6, 149.3, 152.1, 153.1, 155.4. Anal. Calcd. for $C_{26}H_{20}Br_2N_2O$ (536.26): C 58.23, H 3.76, N 5.22; Found: C 58.10, H 3.72, N 5.18%.

14-(3-Bromophenyl)-10,11,12,14-tetrahydro-9H-benzo[5,6]chromeno[2,3-b]-quinolin-13-amine (5i)

Yield 72%; white solid; m.p. > 250 °C. FTIR (KBr) ν 3482, 3348, 2933, 1624, 1439, 1231 cm^{-1} ; 1H NMR: 1.71 (br, 4H, CH_2), 2.21–2.25 (m, 1H, CH_2), 2.37–2.41 (m, 1H, CH_2), 2.53–2.58 (m, 2H, CH_2), 6.08 (s, 2H, NH_2), 6.11 (s, 1H, CH), 7.12–7.16 (t, 1H, $^3J=7.8$ Hz, Ar-H), 7.24–7.26 (m, 1H, Ar-H), 7.41–7.45 (m, 3H, Ar-H), 7.57–7.61 (m, 1H, Ar-H), 7.75 (br, 1H, Ar-H), 7.89–7.92 (m, 2H, Ar-H), 8.29 (d, 1H, $^3J=8.5$ Hz, Ar-H); ^{13}C NMR: 22.5, 22.7, 23.5, 32.3, 35.4, 99.4, 113.2, 117.6, 118.4, 122.2, 123.3, 125.2, 127.1, 127.7, 129.3, 129.9, 130.0, 130.5, 130.9, 131.0, 131.2, 147.6, 149.3, 152.0, 153.2, 155.3; Anal. Calcd. for $C_{26}H_{21}BrN_2O$ (457.36): C 68.28, H 4.63, N 6.12; Found: C 68.31, H 4.57, N 6.16%.

3-Bromo-14-(4-fluorophenyl)-10,11,12,14-tetrahydro-9H-benzo[5,6]chromeno[2,3-b]-quinolin-13-amine (5j)

Yield 87%; white solid; m.p. > 250 °C. FTIR (KBr) ν 3480, 3381, 2929, 1618, 1442, 1233 cm^{-1} ; 1H NMR: 1.70 (br, 4H, CH_2), 2.19–2.23 (m, 1H, CH_2), 2.32–2.37 (m, 1H, CH_2), 2.57 (br, 2H, CH_2), 6.04 (s, 2H, NH_2), 6.12 (s, 1H, CH), 7.00 (t, 2H, $^3J=8.8$ Hz, Ar-H), 7.46–7.50 (m, 3H, Ar-H), 7.70 (dd, 1H, $^3J=6.9, 2.0$ Hz, Ar-H), 7.88 (d, 1H, $^3J=9$ Hz, Ar-H), 8.19 (d, 1H, $^3J=2$ Hz, Ar-H), 8.24 (d, 1H, $^3J=9.1$ Hz, Ar-H); ^{13}C NMR: 22.1, 22.3, 23.1, 32.0, 34.2, 99.8, 111.4, 113.5, 114.6, 115.3, 116.8, 122.0, 124.3, 127.4, 129.0, 129.8, 130.2, 132.6, 131.1, 131.6, 140.5, 148.8, 151.4, 152.2, 154.7. Anal. Calcd. for $C_{26}H_{20}BrFN_2O$ (475.35): C 65.69, H 4.24, N 5.89; Found: C 65.54, H 4.23, N 5.83%.

14-(4-Fluorophenyl)-10,11,12,14-tetrahydro-9H-benzo[5,6]chromeno[2,3-b]-quinolin-13-amine (5k)

Yield 50%; white solid; m.p. > 250 °C. FTIR (KBr) ν 3488, 3354, 2926, 1617, 1439, 1225 cm^{-1} ; 1H NMR: 1.69 (br, 4H, CH_2), 2.20–2.24 (m, 1H, CH_2), 2.38–2.42 (m, 1H, CH_2), 2.57 (br, 2H, CH_2), 6.05 (s, 2H, NH_2), 6.13 (s, 1H, CH), 7.00 (t, 2H, $^3J=8.7$ Hz, Ar-H), 7.38–7.44 (m, 2H, Ar-H), 7.51–7.57 (m, 3H, Ar-H), 7.86–7.90 (m, 2H, Ar-H), 8.32 (d, 1H, $^3J=8.5$ Hz, Ar-H); ^{13}C NMR: 22.1, 22.3, 23.0, 32.0, 34.2, 99.2, 112.3, 114.8, 115.0, 117.80, 117.86, 123.0, 124.3, 126.7, 128.5, 128.8, 129.2, 129.3, 130.2, 130.6, 140.9, 148.8, 151.1, 152.2, 154.8; Anal. Calcd. for $C_{26}H_{21}FN_2O$ (396.46): C 78.77, H 5.34, N 7.06; Found: C 78.84, H, 5.37, N 7.07%.

14-(Thiophen-2-yl)-10,11,12,14-tetrahydro-9H-benzo[5,6]chromeno[2,3-b]quinolin-13-amine (**5f**)

Yield 52%; white solid; m.p. > 250 °C. FTIR (KBr) ν 3464, 3356, 2932, 1622, 1444, 1235 cm^{-1} ; ^1H NMR: 1.72 (br, 4H, CH_2), 2.30–2.32 (m, 1H, CH_2), 2.39–2.43 (m, 1H, CH_2), 2.53–2.58 (m, 2H, CH_2), 6.15 (s, 2H, NH_2), 6.50 (s, 1H, CH), 6.76–6.78 (m, 1H, Ar-H), 7.12–7.15 (m, 2H, Ar-H), 7.39 (d, 1H, $^3J=8.8$ Hz, Ar-H), 7.44 (t, 1H, $^3J=7.2$ Hz, Ar-H), 7.57–7.61 (m, 1H, Ar-H), 7.88–7.93 (m, 2H, Ar-H), 8.40 (d, 1H, $^3J=8.4$ Hz, Ar-H); ^{13}C NMR: 22.1, 22.32, 23.0, 30.6, 32.0, 98.8, 112.2, 117.5, 117.8, 124.2, 125.9, 126.7, 128.4, 128.9, 130.2, 130.7, 148.4, 148.7, 151.3, 152.3, 154.9; Anal. Calcd. for $\text{C}_{24}\text{H}_{20}\text{N}_2\text{OS}$ (384.50): C 74.97, H 5.24, N 7.29 S 8.34; Found: C 74.87, H, 5.21, N 7.24 S 8.29%.

hAChE and hBuChE inhibition assay

Using Ellman's method [67] was measured inhibitory capacity of new compounds on ChE activity. Fresh blood was used to make the enzymes used in this procedure [68]. Synthetic compounds were solved in DMSO and they were then diluted with buffer (0.1 M, pH=8) to reach final concentrations. Phosphate buffer (0.1 M, pH 8, 550 μl), DTNB (3.5 mM, 150 μl), the substrate (acetylthiocholine or butylthiocholine) (7 mM, 150 μl) and different concentrations of inhibitors (150 μl) and phosphate buffer (0.1 M, 700 μl), DTNB (3.5 mM, 150 μl) and different concentrations of inhibitors (150 μl) were dumped in test cuvettes and control cuvettes, respectively. After 5 min, it reached to 37 °C, enzyme (50 μl) was added. All experiments were performed by spectrophotometer Helios-Zeta (Thermospectronic, Cambridge, U.K.) at 412 nm in 5 min.

Kinetic assay

Using Ellman's method, kinetic studies of inhibition on hAChE were performed to obtain the inhibition model and value K_i . In this study, the enzyme relative speed on various concentrations of the substrates (0.1–1 mM) and two various concentrations of inhibitor **5f** (5×10^{-7} – 1×10^{-6} mM) was determined. Linear regression was used for the calculation of Lineweaver–Burk plots, and all Data analysis was done using Microsoft Excel 2013 [69].

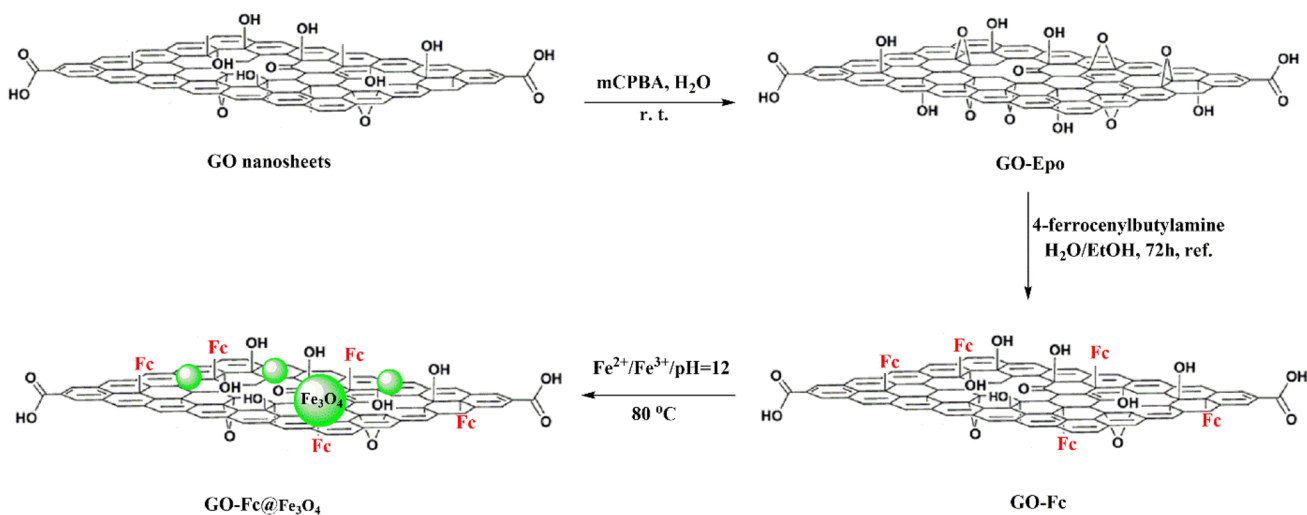
Docking studies

HACHe Structure (pdb ID: 4Ey7) was taken of the Protein Data Bank [70, 71]. To set up and perform blind docking calculations between drug and hAChE were used AutoGrid 4 and AutoDock 4 [72, 73]. At first, water molecules were deleted. Lamarckian genetic algorithms were applied to carry out docking calculations as implemented in AutoDock. The results from AutoDock was rendered with Discovery studio 4.5.

Results and discussion

Synthesis and characterization of GO-Fc@Fe₃O₄ nano hybrid

GO-Fc@Fe₃O₄ nano hybrid as a powerful and reusable nano-catalyst for the synthesis of 2-amino-4H-pyran derivatives was synthesized according to scheme 1. Firstly, over oxidized graphene oxide (GO-Epo) was prepared by the treatment of GO with mCPBA in an aqueous medium at room temperature [63]. This step provides a much reactive site



Scheme 1 Synthesized process of GO-Fc@Fe₃O₄ nano hybrid

for surface modification of GO nanosheets. Afterward, GO-Epo nanosheets were chemically modified with Fc derivative through the ring-opening reaction between GO nanosheets and 4-ferrocenylbutylamine as a nucleophile [60]. Then, Fe_3O_4 nanoparticles were synthesized onto the modified GO surface via a simple co-precipitation of Fe^{2+} and Fe^{3+} under an alkaline solution at 80°C [65]. The final magnetic nanocatalyst denoted as $\text{GO-Fc@Fe}_3\text{O}_4$.

FT-IR spectra of GO, GO-Fc, and $\text{GO-Fc@Fe}_3\text{O}_4$ nanohybrid are depicted in Fig. 2. As shown in Fig. 2, GO nanosheets show several characteristic peaks at about 3400 cm^{-1} , 2900 cm^{-1} , 2800 cm^{-1} , 1700 cm^{-1} , 1600 cm^{-1} which are related to the OH, aromatic C–H bond, aliphatic C–H bond, C=O, and C=C bonds, respectively [74]. As indicated in this figure, in the FT-IR spectrum of GO-Fc, the appearance of a new peak at about 480 cm^{-1} can be assigned to the Fe–Cp bond in Fc rings. This new peak proved the success of the grafting of Fc groups onto GO nanosheets. Also, the FT-IR spectrum of $\text{GO-Fc@Fe}_3\text{O}_4$ nanohybrid exhibits a strong IR peak at around 570 cm^{-1} which is related to the stronger bending vibration of Fe–O in Fe_3O_4 nanoparticles [75]. These findings indicate that the Fe_3O_4 nanoparticles were successfully synthesized by the in situ nanoparticle growth method onto the GO-Fc surface.

The XRD patterns of GO, GO-Fc, $\text{GO-Fc@Fe}_3\text{O}_4$ nanohybrid are shown in Fig. 3. The XRD pattern of GO exhibits a sharp diffraction peak at $2\theta = 11.5^\circ$ which is attributed to the (001) peak ($d \sim 0.77\text{ nm}$). After modification of GO surface with Fc moieties, the XRD peak position and shape of GO-Fc changes compared to the XRD peak of GO. These changes may be due to the presence of Fc rings onto the GO surface which disrupts the crystalline structure of GO nanosheets.

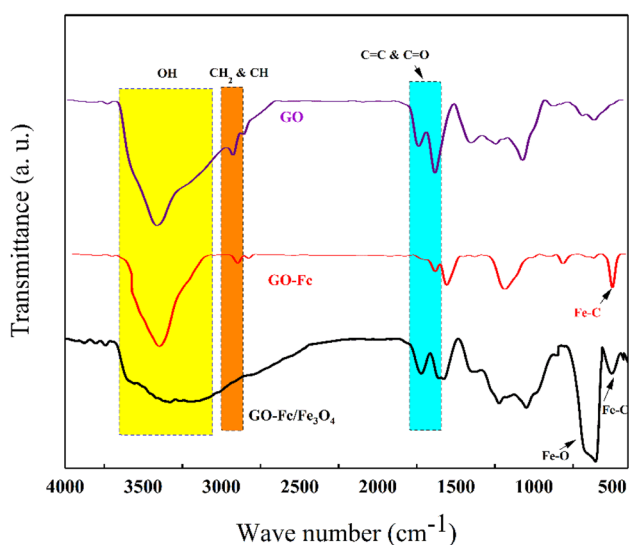


Fig. 2 FT-IR spectra of GO, GO-Fc, $\text{GO-Fc@Fe}_3\text{O}_4$ nanohybrid

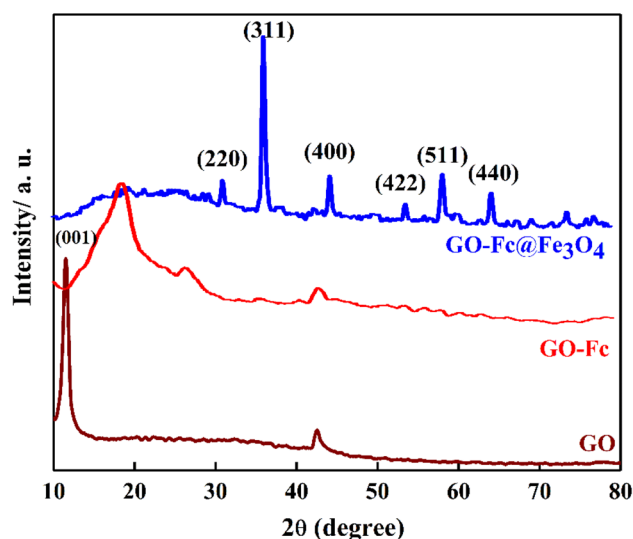


Fig. 3 XRD patterns of GO, GO-Fc, $\text{GO-Fc@Fe}_3\text{O}_4$ nanohybrid

The XRD pattern of $\text{GO-Fc@Fe}_3\text{O}_4$ nanohybrid confirmed the presence of Fe_3O_4 nanoparticles and GO-Fc nanosheets related diffraction peaks. Broad XRD peaks of $\text{GO-Fc@Fe}_3\text{O}_4$ nanohybrid compared to GO-Fc nanosheets can be attributed to the growth of Fe_3O_4 nanoparticles between GO layers.

FE-SEM micrographs of GO, GO-Fc, $\text{GO-Fc@Fe}_3\text{O}_4$ nanohybrid are depicted in Fig. 4 that tangible changes are observed in the FE-SEM micrographs of them. The FE-SEM image of GO (Fig. 4a) exhibits a layered structure with wrinkles visible. The wrinkled structure of GO can be due to the presence of oxygenic functional groups on its surface. After modification of GO surface with Fc moieties, the GO-Fc nanosheets show rich-wrinkle morphology and also are increased surface turbidity that is due to the entry of Fc into the GO surface (Fig. 4b). Also the presence of aggregated nearly spherical Fe_3O_4 nanoparticles on the GO-Fc surface is shown in Fig. 4c. FE-SEM images demonstrate that the $\text{GO-Fc@Fe}_3\text{O}_4$ nanohybrid was successfully synthesized. Furthermore, the EDX analysis of $\text{GO-Fc@Fe}_3\text{O}_4$ nanohybrid shows the elements in the structure of nanocatalyst.

EDX analysis is a powerful tool for evaluating the elements of the synthesized compounds. From EDX curves (Fig. 5), they are confirmed that the related elements of GO including C and O were present in the synthesized GO (Fig. 5a). The EDX analysis of the over-oxidized form of GO (GO-Epo) shows a significant increase of O element (Fig. 5b). The presence of the abundance of epoxy rings on the GO surface provides an option of using these active sites for the covalently grafted of Fc moieties on the GO surface through ring-opening reaction. The presence of Fe element in the EDX analysis of GO-Fc (Fig. 5c) confirms the successful modification of GO-Epo surface with Fc moieties.

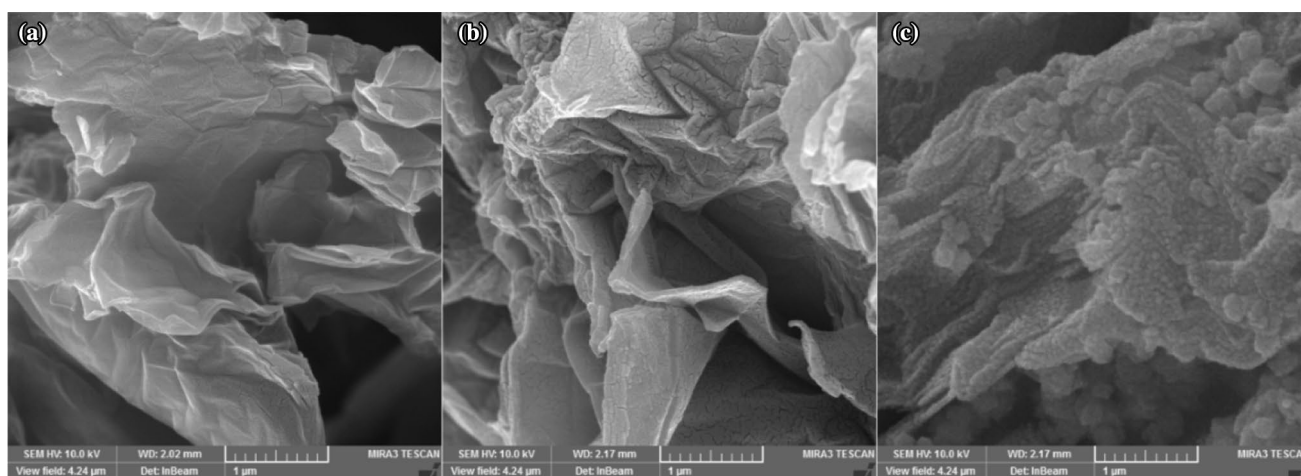


Fig. 4 FE-SEM images of **a** GO, **b** GO-Fc, **c** GO-Fc@Fe₃O₄ nanohybrid

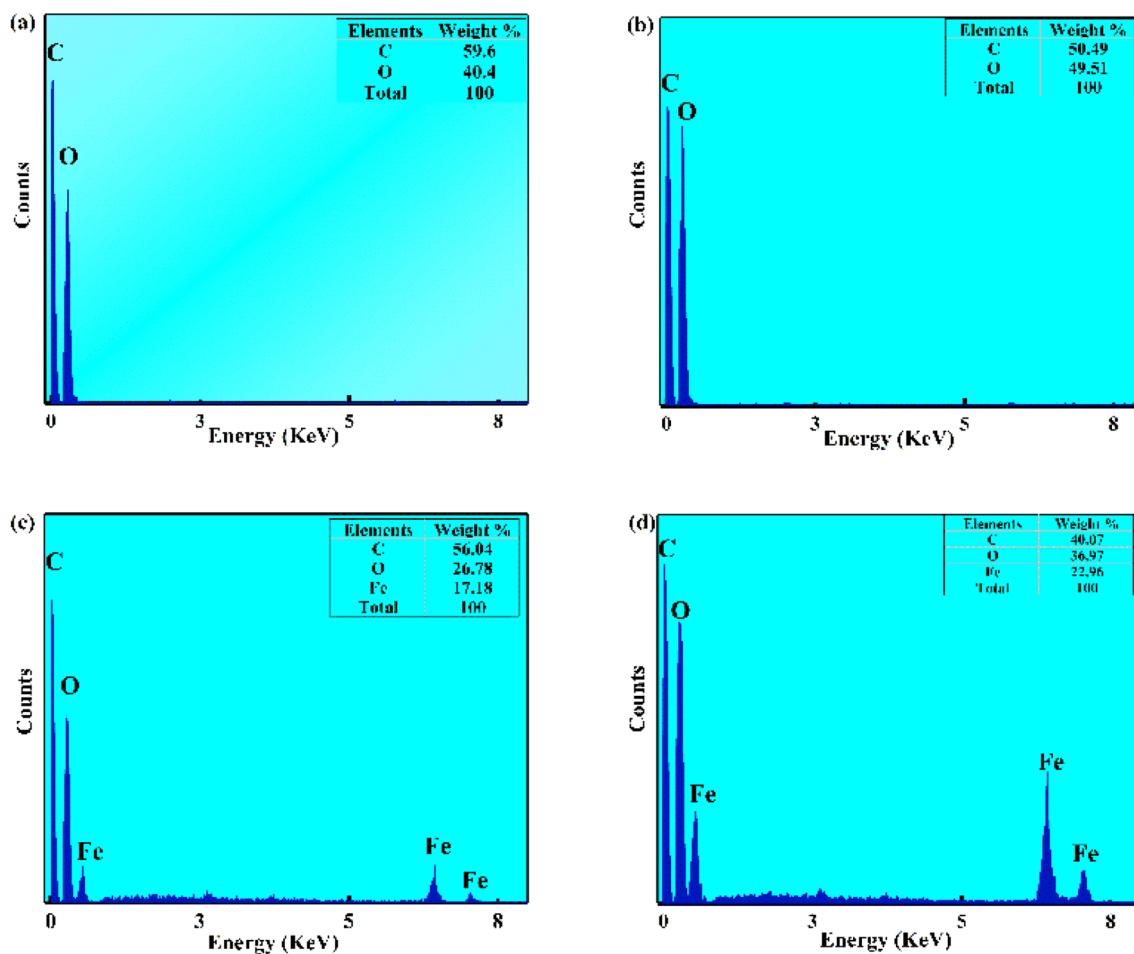


Fig. 5 EDX curves of **a** GO, **b** GO-Epo, **c** GO-Fc, **d** GO-Fc@Fe₃O₄ nanohybrid

The EDX analysis of GO-Fc@Fe₃O₄ nanohybrid (Fig. 5d) confirms that the Fe₃O₄ nanoparticles are successfully grown onto GO layers.

Also, the magnetic properties of GO-Fc@Fe₃O₄ nanocatalyst have been studied by vibrating sample magnetometer (VSM) technique at room temperature (Fig. 6). As shown

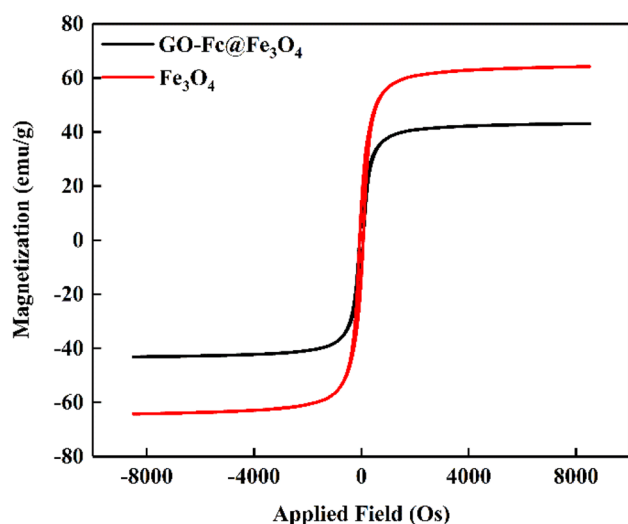


Fig. 6 Magnetic hysteresis loop of Fe_3O_4 and $\text{GO-Fc@Fe}_3\text{O}_4$ nanohybrid

in Fig. 6, the saturation magnetization (M_s) values of Fe_3O_4 and $\text{GO-Fc@Fe}_3\text{O}_4$ nanohybrid are 64 emu/g and 43 emu/g, respectively. The saturation magnetization value is decreased due to the intercalation of Fe_3O_4 nanoparticles into GO-Fc layers. However, the $\text{GO-Fc@Fe}_3\text{O}_4$ nanocatalyst exhibited enough magnetization value that can be easily separated from the reaction mixture by an external magnet.

Catalytic test of $\text{GO-Fc@Fe}_3\text{O}_4$ nanohybrid

To check the catalytic performance of the $\text{GO-Fc@Fe}_3\text{O}_4$ nanohybrid, firstly, a model reaction between 2-naphthol (**1a**), benzaldehyde (**2a**), and malononitrile (**3**) was chosen. According to previous studies, the presence of acidic and basic sites in the synthesized nanocatalyst can facilitate a coupling reaction between the above mentioned three components [51, 76–78]. Also, based on the catalytic activity of Fc, $\text{GO-Fc@Fe}_3\text{O}_4$ nanohybrid has several acidic and

basic sites including carboxylic acid, hydroxyl, Fc rings on the GO-Fc surface (Fig. 7). Also, GO nanosheets provide a large available surface area. These mentioned reasons can promote the formation of desired products.

To determine the optimum reaction conditions, the model reaction was performed under various conditions including various solvents, temperature, and amount of catalyst (Table 1). At first, the model reaction was carried out in various solvents and solvent-free systems in the presence of 40 mg of synthesized nanocatalyst at ambient temperature (Table 1, Entries 1–4). Among these conditions, the best yield was achieved under solvent-free conditions. Afterwards, the influence of catalyst amount and various temperature on the yield of the model reaction was investigated by using different amounts of the synthesized nanocatalyst (40, 30, 20, 10, and 5 mg) in the model reaction. As indicated in Table 1, the best results were obtained during 40 min under solvent-free conditions at 100 °C in the presence of 10 mg of the magnetic synthesized nanocatalyst (Entry 13).

After finding the optimum conditions, to explore the catalytic activity, the reaction between 2-naphthol (**1a**) and 6-bromo-2-naphthol (**1b**) with various aromatic aldehydes (**2a–j**), and malononitrile (**3**) (Scheme 2) were tested under optimum conditions (Table 2). Moreover, the existence of electron-donating and electron-withdrawing functional groups on the aromatic aldehyde ring has no remarkable difference in the yield of the reactions. These findings demonstrate the higher activity of the synthesized nanocatalyst.

Finally, we tested the recyclability of $\text{GO-Fc@Fe}_3\text{O}_4$ as a magnetic nanocatalyst for the coupling of three components in the model reaction. Upon completion of the reaction, the crude product was dissolved in hot ethanol and the magnetic nanocatalyst was separated using an external magnet. Then, the separated magnetic nanocatalyst was washed several times with hot ethanol and dried. The recovered magnetic nanocatalyst can be reused 7 times without any significant changes in reaction yield (Fig. 8).

Fig. 7 Schematic presentation of the synthesized nanocatalyst

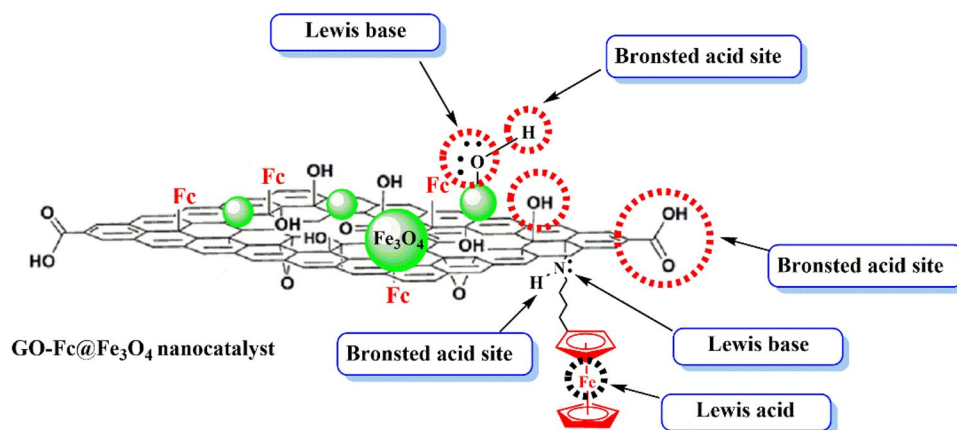
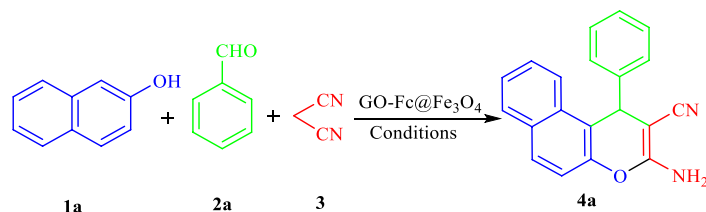
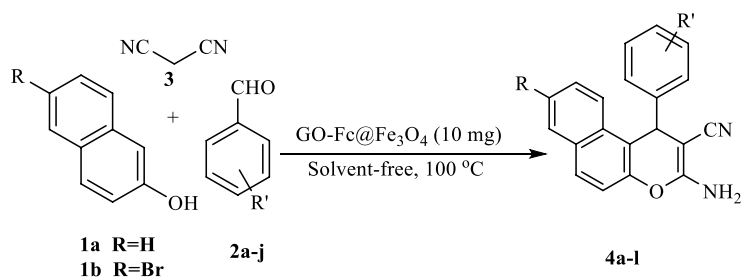


Table 1 Determining the optimum reaction conditions

Entry	Catalyst amount (mg)	Solvent	Temperature (°C)	Time (min)	Yield (%)
1	–	–	r.t	120	Trace
2	40	EtOH	r. t.	110	18
3	40	MeOH	r. t.	110	22
4	40	H ₂ O	r. t.	110	9
5	40	–	r. t.	110	42
6	30	–	r. t.	80	40
7	20	–	r. t.	80	40
8	10	–	r. t.	80	40
9	5	–	r. t.	80	33
10	10	–	50	80	51
11	10	–	70	50	63
12	10	–	80	45	70
13	10	–	90	45	79
14	10	–	100	40	83
15	10	–	110	45	81

Reaction conditions: 2-naphthol/benzaldehyde/malononitrile = 1:1:1.2

Scheme 2 Synthesis of 2-amino-3-cyano-4*H*-pyran derivatives (**4a–l**) under optimum conditions



We propose a possible mechanism of GO-Fc@Fe₃O₄ catalyzed reaction as depicted in scheme 3. After activation of the aldehyde groups, a Knoevenagel condensation was carried out between aromatic aldehyde and malononitrile, and arylidenemalononitrile was formed as intermediate. Afterward, the arylidenemalononitrile was coupled with 2-naphthol through Michael's addition reaction followed by electrophilic cyclization to form the desired product [70].

Preparation of tacrine-naphthopyran hybrid derivatives (**5a–l**)

14-Aryl-10,11,12,14-tetrahydro-9*H*-benzo[5,6]chromeno[2,3-*b*]-quinolin-13-amines (**5a–l**) as new tacrine

hybrids analogs and hAChE inhibitors have been synthesized by the AlCl₃ promoted Friedländer-type reaction between 2-amino-3-cyano-4*H*-pyrans derivatives (**4a–l**) and cyclohexanone as the selected ketone in dry 1,2-dichloroethane (DCE) at 83 °C, in good yields (50–92%) (Scheme 4) [26, 66].

hAChE inhibition

One way to treat AD is inhibition of ChE enzymes. The cholinesterase inhibition activity of compounds **4a–l** and compounds **5a–l** was investigated in vitro and using Ellman's spectrophotometric method against hAChE and hBuChE [67]. Fresh blood was used to prepare the enzymes

Table 2 Synthesis of 2-amino-3-cyano-4*H*-pyran derivatives

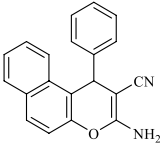
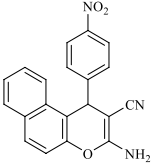
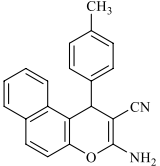
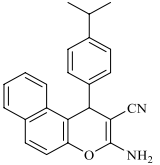
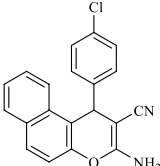
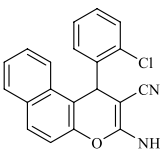
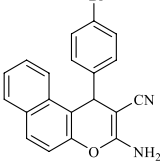
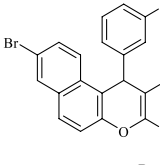
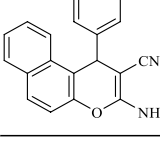
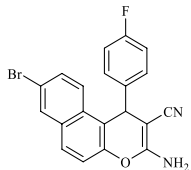
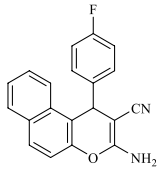
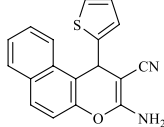
Entry	Product	Structure	Time (min)	Yield (%)	Obs. M.p. (°C)	Lit. M.p. (°C)
1	4a		40	83	278–281	279–282 [51]
2	4b		25	75	186–189	183–185 [51]
3	4c		35	75	271–274	270–273 [76]
4	4d		40	73	217–219	218–220 [76]
5	4e		25	80	206–209	207–209 [76]
6	4f		30	69	269–272	271–272 [77]
7	4g		25	78	210–213	212–215 [76]
8	4h		35	70	197–201	198–201 [78]
9	4i		35	68	221–225	224–227 [78]

Table 2 (continued)

Entry	Product	Structure	Time (min)	Yield (%)	Obs. M.p. (°C)	Lit. M.p. (°C)
10	4j		20	65	256–260	258–262 [78]
11	4k		25	70	228–232	228–229 [77]
12	4l		40	50	256–259	258–260 [78]

[68]. The amount of inhibition of compounds **4a–l** against hAChE and hBuChE was not sufficient to obtain IC_{50} for them and these compounds did not show inhibitory activity. Tacrine and galantamine are used as a positive control and the outcome was illustrated as IC_{50} amount of synthesized compounds in Table 3. The obtained results have shown that compounds **5a–l** had medium inhibition activity of hAChE at micro-molar. However, the amount of inhibition of these compounds (**5a–l**) for hBuChE was not sufficient to obtain IC_{50} for them and it can be said that these compounds do not

show hBuChE inhibitory activity. The range of IC_{50} values was obtained from 0.16 μ M to 37.48 μ M for hAChE. Among them, compound **5f** with IC_{50} value equal 0.16 μ M displayed good inhibitory activity against hAChE which shows more inhibitory activity of tacrine and galantamine.

Kinetic analysis

The mechanism of hAChE inhibition for compounds **5a–l** was investigated using compound **5f**. So, kinetic studies of compound **5f** as a representative compound with the greatest inhibit hAChE activity between other synthesized compounds was carried out to characterize a better understanding of the mechanism of enzyme inhibition. Due to the structural similarity of the synthesized compounds, a similar practical method was predicted. Using the Lineweaver–Burk plots was determined the type of inhibition (Fig. 9). According to the results, compound **5f** was showed mixed-type inhibition. This analysis gives inhibition constants with K_i value equal to 0.8 μ M and K_I value equal to 0.3 μ M. According to available reports, compound **5f** is presumably binding simultaneously to the CAS and PAS of hAChE [17, 22].

Molecular docking

The use of computational methods is interest to design new compounds nowadays and the use of molecular docking studies can be obtained interaction affinity between molecules and hAChE enzyme. So, molecular docking studies on the selective compound **5f** was performed, to get more information of interact with hAChE on their active site. According to the results, the derivatives can inhibit the enzyme, by binding to the active site of hAChE. The results obtained from the docking

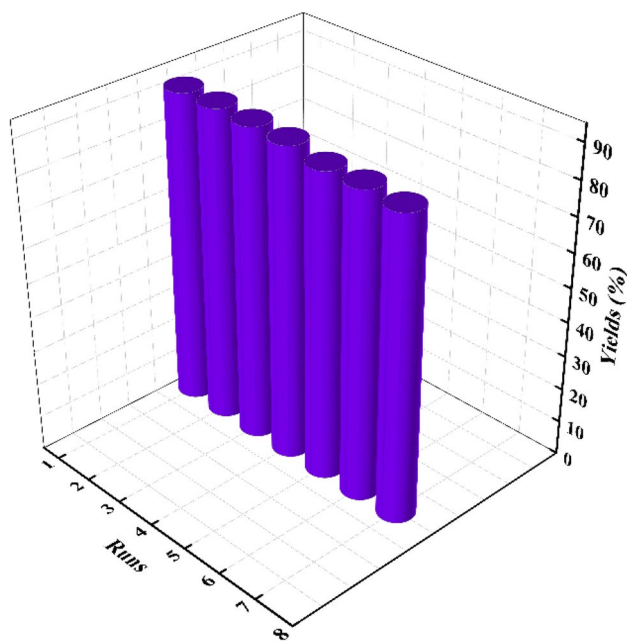
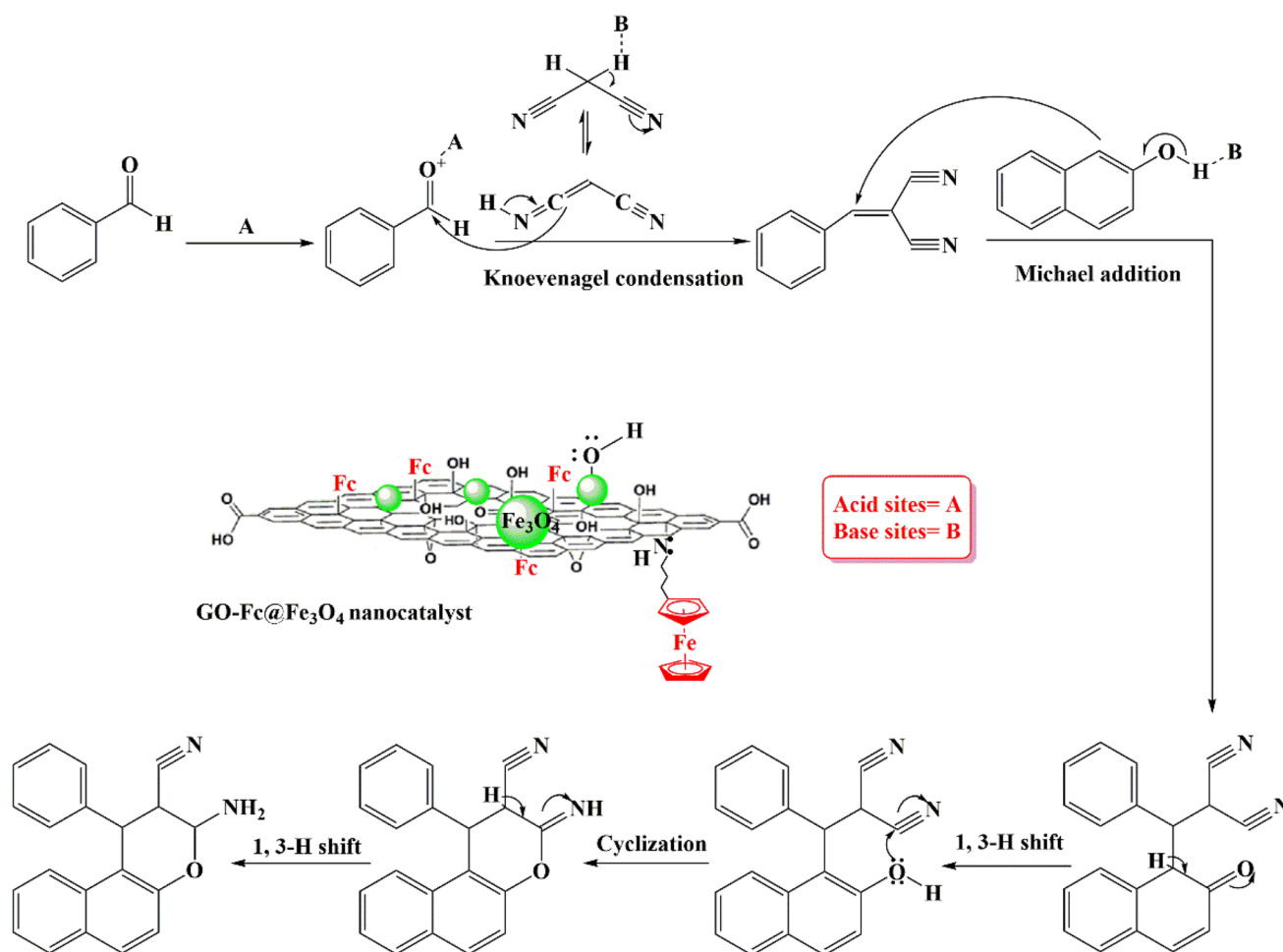
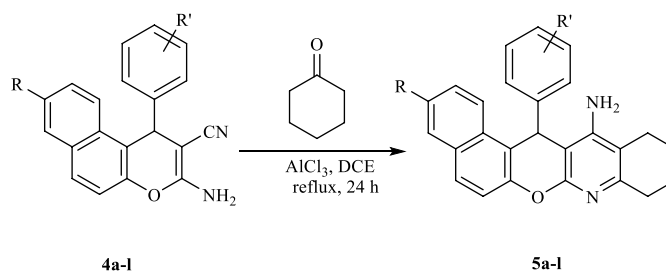


Fig. 8 Reusability of GO-Fc@Fe₃O₄ nanocatalyst during 7 runs



Scheme 4 Preparation of tacrine-naphthopyran hybrid derivatives (**5a-l**)



of compound **5f** (Fig. 10) show that this compound has a better interaction than tacrine (Fig. 11). The binding energy get for compound **5f** and tacrine was equal to -11.61 kcal/mol and -7.17 kcal/mol, respectively. The compound of **5f** and tacrine do not show any hydrogen bonding. The results showed tacrine interacted with TYR341, PHE338, PHE295, TYR124, SER293, TRP286, and VAL294. So, the results were obtained for compound **5f** show that TRP86, GLY448, SER203, HIS447, and TYR337 placed around of naphthopyran moiety, GLY121, ASP74 and SER125 are around of 2-Cl-ph and

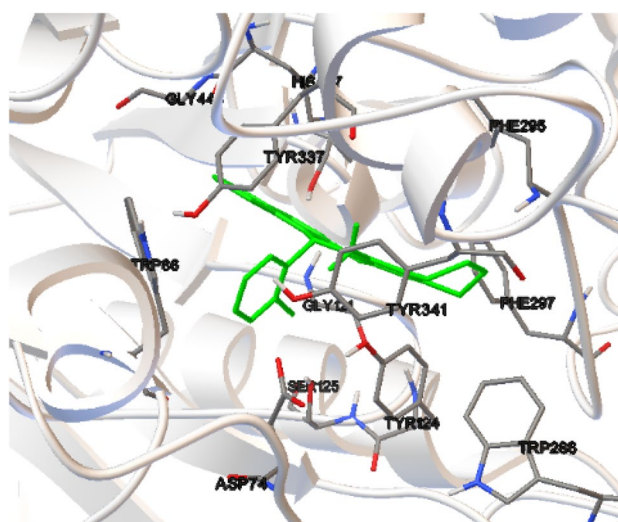
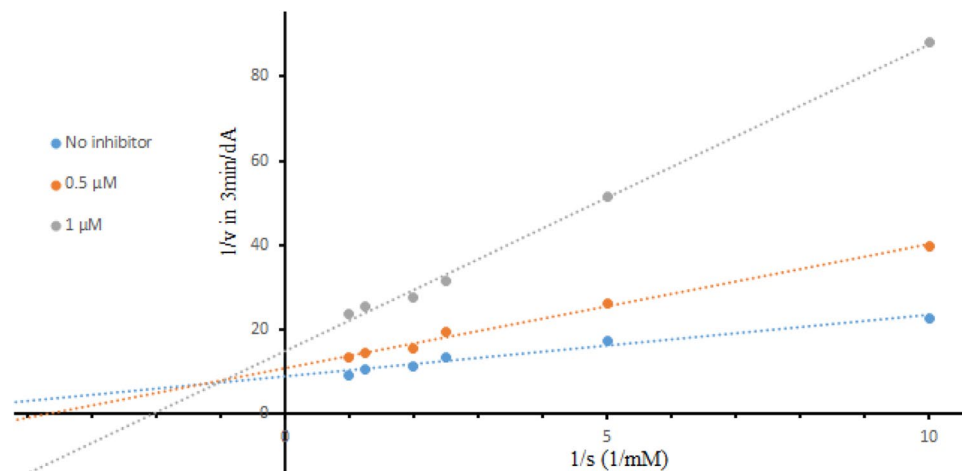
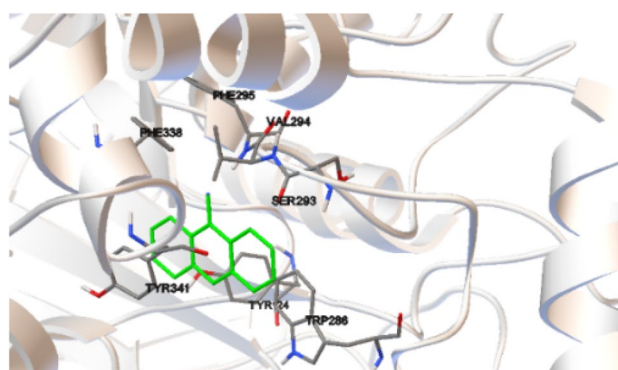
PHE297, PHE295, TYR124, TYR341, and TRP286 placed around of 5,6,7,8-tetrahydroquinolin-4-amine moiety. The compound **5f** interacted with the peripheral anionic site (PAS) and catalytic active site (CAS) of hAChE.

Table 3 IC₅₀ (μM) values for inhibitory activity of hAChE by the synthesized tacrine-naphthopyran hybrid derivatives (**5a–l**)

Entry	Product	R	R'	hAChE (μM)
1	5a	H	H	4.25 ± 0.32
2	5b	H	4-NO ₂	37.48 ± 1.33
3	5c	H	4-CH ₃	10.95 ± 1.03
4	5d	H	(CH ₃) ₂ CH	12.23 ± 0.67
5	5e	H	4-Cl	2.03 ± 0.4
6	5f	H	2-Cl	0.16 ± 0.07
7	5g	H	4-Br	2.66 ± 0.32
8	5h	Br	3-Br	1.69 ± 0.11
9	5i	H	3-Br	0.23 ± 0.2
10	5j	Br	4-F	25.60 ± 1.03
11	5k	H	4-F	29.31 ± 1.23
12	5l	H	2-Thiophene	8.02 ± 0.71
13	Tacrine	–	–	0.19 ± 0.05
14	Galantamine	–	–	3 ± 0.18

Conclusion

In summary, the chemically modified GO-Epo by Fc moiety was synthesized successfully. Then, the novel GO-Fc@Fe₃O₄ nanohybrid was formed by synthesized of Fe₃O₄ nanoparticles onto the GO-Fc sheets. Various analyses such as FT-IR, FESEM, EDX, XRD, and VSM analysis were used for the evaluation of all of the intermediates to final nanocatalyst. GO-Fc@Fe₃O₄ nanohybrid was used as an efficient heterogeneous catalyst for the synthesis 2-amino-3-cyano-4*H*-pyran derivatives (**4a–l**). Also, the results of its catalytic activity investigation showed that the presence of acidic and basic sites in the synthesized nanocatalyst increased catalytic activity in this reaction. The relative simplicity of separation, high yields, recyclability and reusability are the advantages of using

Fig. 9 Lineweaver–Burk plots of hAChE inhibition kinetic of compound **5f****Fig. 10** Compound **5f** interaction with hAChE**Fig. 11** Tacrine interaction with hAChE

GO-Fc@Fe₃O₄ as a catalyst in this multi-component reaction. Also, 14-aryl-10,11,12,14-tetrahydro-9*H*-benzo[5,6]chromeno[2,3-*b*]-quinolin-13-amines derivatives (**5a–l**)

were synthesized as tacrine-naphthopyran hybrid derivatives by Friedländer reaction between compounds **4a–l** and cyclohexanone. In the following, in vitro anti-hAChE and anti-hBuChE inhibitory activities of compounds **5a–l** were investigated. These compounds showed selectively good inhibition of hAChE and among them, compound **5f** was a stronger inhibitor of hAChE with IC₅₀ value equal to 0.16 μM. But these series did not show any inhibition for hBuChE.

Acknowledgements The authors would like to acknowledge the financial support from Iran National Science Foundation (INSF) (To Project Number: 97015588), Health Ministry of Islamic Republic of Iran, Tabriz University of medical sciences and the University of Tabriz.

References

1. S. Mozaffarnia, F. Parsaee, E. Payami, H. Karami, S. Soltani, M.R. Rashidi, R. Teimuri-Mofrad, *ChemistrySelect* **4**, 9376 (2019)
2. K. Czarnecka, M. Girek, K. Maciejewska, R. Skibiński, J. Jończyk, M. Bajda, J. Kabziński, P. Sołowiej, I. Majsterek, P. Szymański, *J. Enzyme Inhib. Med. Chem.* **33**, 158 (2018)
3. L. Peauger, R. Azzouz, V. Gembus, M.L. Tintas, J. Sopková-de Oliveira Santos, P. Bohn, C. Papamicaël, V. Levacher, *J. Med. Chem.* **60**, 5909 (2017)
4. S. Mozaffarnia, R. Teimuri-Mofrad, M.-R. Rashidi, *Eur. J. Med. Chem.* **191**, 112140 (2020)
5. A. Dorababu, *Bioorg. Chem.* **93**, 103299 (2019)
6. C. Zhang, Q.-Y. Du, L.-D. Chen, W.-H. Wu, S.-Y. Liao, L.-H. Yu, X.-T. Liang, *Eur. J. Med. Chem.* **116**, 200 (2016)
7. X. Zhang, X. He, Q. Chen, J. Lu, S. Rapposelli, R. Pi, *Bioorg. Med. Chem.* **26**, 543 (2018)
8. L. Monjas, M.P. Arce, R. León, J. Egea, C. Pérez, M. Villarroya, M.G. López, C. Gil, S. Conde, M.I. Rodríguez-Franco, *Eur. J. Med. Chem.* **130**, 60 (2017)
9. R. Azzouz, L. Peauger, V. Gembus, M.-L. Tintás, J. Sopková-de Oliveira Santos, C. Papamicael, V. Levacher, *Eur. J. Med. Chem.* **145**, 165 (2018)
10. Z.-Q. Cheng, K.-K. Zhu, J. Zhang, J.-L. Song, L.A. Muehlmann, C.-S. Jiang, C.-L. Liu, H. Zhang, *Bioorg. Chem.* **83**, 277 (2019)
11. K.S.T. Dias, C.T. de Paula, T. dos Santos, I.N. Souza, M.S. Boni, M.J. Guimarães, F.M. da Silva, N.G. Castro, G.A. Neves, C.C. Veloso, M.M. Coelho, *Eur. J. Med. Chem.* **130**, 440 (2017)
12. M. Eghtedari, Y. Sarrafi, H. Nadri, M. Mahdavi, A. Moradi, F.H. Moghadam, S. Emami, L. Firoozpour, A. Asadipour, O. Sabzevari, A. Foroumadi, *Eur. J. Med. Chem.* **128**, 237 (2017)
13. H. Farrokhi, S. Mozaffarnia, K. Rahimpour, M.R. Rashidi, R. Teimuri-Mofrad, *J. Iran. Chem.* **17**, 593 (2020)
14. Z. Haghghijoo, O. Firuzi, B. Hemmateenejad, S. Emami, N. Edraki, R. Miri, *Bioorg. Chem.* **74**, 126 (2017)
15. M. Shidore, J. Machhi, K. Shingala, P. Murumkar, M.K. Sharma, N. Agrawal, A. Tripathi, Z. Parikh, P. Pillai, M.R. Yadav, *J. Med. Chem.* **59**, 5823 (2016)
16. E. Sawatzky, S. Wehle, B. Kling, J. Wendrich, G. Bringmann, C.A. Sotriffer, J. Heilmann, M. Decker, *J. Med. Chem.* **59**, 2067 (2016)
17. J.-S. Lan, T. Zhang, Y. Liu, J. Yang, S.-S. Xie, J. Liu, Z.-Y. Miao, Y. Ding, *Eur. J. Med. Chem.* **133**, 184 (2017)
18. A. Iraj, M. Khoshneviszadeh, O. Firuzi, M. Khoshneviszadeh, N. Edraki, *Bioorg. Chem.* **97**, 103649 (2020)
19. H.J. Tseng, M.H. Lin, Y.J. Shiao, Y.C. Yang, J.C. Chu, C.Y. Chen, Y.Y. Chen, T.E. Lin, C.J. Su, S.L. Pan, L.C. Chen, *Eur. J. Med. Chem.* **192**, 112193 (2020)
20. J. Li, L. Zhang, D. Shi, Q. Li, D. Wang, C. Wang, Q. Zhang, L. Zhang, Y. Fan, *Synlett* **2**, 233 (2008)
21. J. Korábečný, E. Nepovimova, T. Cikankova, K. Špilovská, L. Vašková, E. Mezeiova, K. Kuča, J. Hroudova, *Neuroscience* **370**, 191 (2018)
22. A. McEneny-King, W. Osman, A.N. Edginton, P.P. Rao, *Bioorg. Med. Chem. Lett.* **27**, 2443 (2017)
23. M. Esquivias-Pérez, E. Maalej, A. Romero, F. Chabchoub, A. Samadi, J. Marco-Contelles, M.J. Oset-Gasque, *Chem. Res. Toxicol.* **26**, 986 (2013)
24. H. Boulebd, L. Ismaili, H. Martin, A. Bonet, M. Chioua, J. Marco Contelles, A. Belfaitah, *Future Med. Chem.* **9**, 723 (2017)
25. C. Derabli, I. Boualia, A.B. Abdelwahab, R. Boulcina, C. Bensouici, G. Kirsch, A. Debache, *Med. Chem. Lett.* **28**, 2481 (2018)
26. M. Khoobi, F. Ghanoni, H. Nadri, A. Moradi, M.P. Hamedani, F.H. Moghadam, S. Emami, M. Vosoughi, R. Zadmand, A. Foroumadi, A. Shafiee, *Eur. J. Med. Chem.* **89**, 296 (2015)
27. J.M. Roldan-Pena, D. Alejandro-Ramos, O. Lopez, I. Maya, I. Lagunes, J.M. Padron, L.E. Pena-Altamira, M. Bartolini, B. Monti, M.L. Bolognesi, J.G. Fernandez-Bolanos, *Eur. J. Med. Chem.* **138**, 761 (2017)
28. M. Shiri, M.A. Zolfigol, H.G. Kruger, Z. Tanbakouchian, *Adv. Heterocycl. Chem.* **102**, 139 (2011)
29. W.S. Hamama, S.M. Waly, S.B. Said, H.H. Zoorob, *J. Heterocycl. Chem.* **55**, 1554 (2018)
30. J. Quiroga, J. Trilleras, R. Abonía, B. Insuasty, M. Noguera, J. Cobo, J.M. de la Torre, *Arkivoc* (2009). <https://doi.org/10.3998/ark.5550190.0010.e02>
31. D. Kumar, V.B. Reddy, S. Sharad, U. Dube, S. Kapur, *Eur. J. Med. Chem.* **44**, 3805 (2009)
32. J. Jung, B.H. Park, Y.R. Lee, *Green Chem.* **12**, 2003 (2010)
33. S. Banerjee, A. Horn, H. Khatri, G. Sereda, *Tetrahedron Lett.* **52**, 1878 (2011)
34. M. Gholamhosseini-Nazari, S. Esmati, K.D. Safa, A. Khataee, R. Teimuri-Mofrad, *Appl. Organomet. Chem.* **33**, e4701 (2019)
35. A.H.F. Abd El-Wahab, *Pharmaceuticals* **5**, 745 (2012)
36. N.J. Thumar, M.P. Patel, *Arkivoc* **13**, 363 (2009)
37. Y. Essamlali, O. Amadine, H. Maati, K. Abdelouahdi, A. Fihri, M. Zahouily, R.S. Varma, A. Solhy, *ACS Sustain. Chem. Eng.* **1**, 1154 (2013)
38. M. Frigoli, F. Maurel, J. Berthet, S. Delbaere, J. Marrot, M.M. Oliveira, *Org. Lett.* **14**, 4150 (2012)
39. P.J.J. Huang, T.S. Cameron, A. Jha, *Tetrahedron Lett.* **50**, 51 (2009)
40. A.A. Hussein, I. Barberena, T.L. Capson, T.A. Kursar, P.D. Coley, P.N. Solis, M.P. Gupta, *J. Nat. Prod.* **67**, 451 (2004)
41. T.S. Jin, J.S. Zhang, L.B. Liu, A.Q. Wang, T.S. Li, *Synth. Commun.* **36**, 2009 (2006)
42. A.V. Karnik, A.M. Kulkarni, N.J. Malviya, B.R. Mourya, B.L. Jadhav, *Eur. J. Med. Chem.* **43**, 2615 (2008)
43. S. Li, Y. Yao, Z. Tang, B. Sun, C. Yu, T. Li, C. Yao, *Org. Biomol. Chem.* **17**, 268 (2019)
44. S. Verma, S.L. Jain, *Tetrahedron Lett.* **53**, 6055 (2012)
45. H. Yarahmadi, H.R. Shaterian, *J. Chem. Res.* **36**, 49 (2012)
46. P. Anastas, N. Eghbali, *Chem. Soc. Rev.* **39**, 301 (2010)
47. R. Teimuri-Mofrad, S. Esmati, S. Tahmasebi, M. Gholamhosseini-Nazari, *J. Organomet. Chem.* **870**, 38 (2018)
48. R. Teimuri-Mofrad, S. Esmati, M. Rabiei, M. Gholamhosseini-Nazari, *J. Chem. Res.* **42**, 7 (2018)
49. R. Mohammadi, S. Esmati, M. Gholamhosseini-Nazari, R. Teimuri-Mofrad, *J. Mol. Liq.* **275**, 523 (2019)
50. R. Mohammadi, S. Esmati, M. Gholamhosseini-Nazari, R. Teimuri-Mofrad, *New J. Chem.* **43**, 135 (2019)

51. M. Tajbakhsh, M. Kariminasab, H. Alinezhad, R. Hosseinzadeh, P. Rezaee, M. Tajbakhsh, H.J. Gazvini, M.A. Amiri, J. Iran. Chem. Soc. **12**, 1405 (2015)
52. J. Raktshah, B. Shaabani, S. Salehzadeh, N. Hosseinpour Moghadam, Bioorg. Chem. **85**, 420–430 (2019)
53. J. Raktshah, F. Yaghoobi, Int. J. Biol. Macromol. **139**, 904–916 (2019)
54. S. Rostamnia, E. Doustkhah, J. Magn. Magn. Mater. **386**, 111–116 (2015)
55. D. Yuan, L. Chen, L. Yuan, S. Liao, M. Yang, Q. Zhang, Chem. Eng. J. **287**, 241–251 (2016)
56. A. Ghorbani-Choghamarani, B. Ghasemi, Z. Safari, G. Azadi, Catal. Commun. **60**, 70–75 (2015)
57. R. Teimuri-Mofrad, Sh Tahmasebi, E. Payami, Appl. Organomet. Chem. **33**, e4773 (2019)
58. R. Teimuri-Mofrad, H. Abbasi, K.D. Safa, B. Tahmasebi, Arkivoc **4**, 371 (2016)
59. C. Liu, F. Su, J. Liang, Appl. Surf. Sci. **351**, 889 (2015)
60. R. Teimuri-Mofrad, E. Payami, I. Ahadzadeh, Electrochim. Acta **321**, 134706 (2019)
61. S. Park, J. An, J.R. Potts, A. Velamakanni, S. Murali, R.S. Ruoff, Carbon **49**, 3019 (2011)
62. W.S. Hummers Jr., R.E. Offeman, J. Am. Chem. Soc. **80**, 1339 (1958)
63. K.C. Mei, N. Rubio, P.M. Costa, H. Kafa, V. Abbate, F. Festy, S.S. Bansal, R.C. Hider, K.T. Al-Jamal, Chem. Commun. **51**, 14981 (2015)
64. R. Teimuri-Mofrad, H. Abbasi, T. Vahedinia, I. Ahadzadeh, J. Inorg. Organomet. Polym Mater. **30**, 955 (2020)
65. M. Heidarizadeh, E. Doustkhah, S. Rostamnia, P.F. Rezaei, F.D. Harzevili, B. Zeynizadeh, Int. J. Biol. Macromol. **101**, 696–702 (2017)
66. E. Maalej, F. Chabchoub, A. Samadi, C. Rios, A. Perona, A. Morreale, J. Marco-Contelles, Bioorg. Med. Chem. Lett. **21**, 2384 (2011)
67. G.L. Ellman, K.D. Courtney, V.J. Andres, R.M. Fesrtherstone, Biochem. Pharmacol. **7**, 88 (1961)
68. G. Karimi, M. Iranshahi, F. Hosseinalizadeh, B. Riahi, A. Sahebkar, Pharmacologyonline **1**, 566 (2010)
69. A. Rampa, A. Bisi, F. Belluti, S. Gobbi, P. Valenti, V. Andrisano, V. Cavrini, A. Cavalli, M. Recanatini, Bioorg. Med. Chem. **8**, 497 (2000)
70. <https://www.rcsb.org/structure/4EY7>
71. Y. Nicolet, O. Lockridge, P. Masson, J.C. Fontecilla-Camps, F. Nachon, J. Biol. Chem. **278**, 41141 (2003)
72. G.M. Morris, R. Huey, W. Lindstrom, M.F. Sanner, R.K. Belew, D.S. Goodsell, A.J. Olson, J. Comput. Chem. **30**, 2785 (2009)
73. G.M. Morris, R. Huey, A.J. Olson, Curr. Protoc. Bioinform. **1**, 8 (2008)
74. Q. Zhang, Y. Li, Y. Feng, W. Feng, Electrochim. Acta **90**, 95 (2013)
75. Y. Li, H. Lu, Y. Wang, Y. Zhao, X. Li, J. Mater. Sci. **54**, 7603 (2019)
76. R. Teimuri-Mofrad, M. Gholamhosseini-Nazari, E. Payami, S. Esmati, Appl. Organomet. Chem. **32**, e3955 (2018)
77. A.R. Moosavi-Zare, M.A. Zolfigol, O. Khaledian, V. Khakyzadeh, M. Darestani Farahani, M.H. Beyzavi, H.G. Kruger, Chem. Eng. J. **248**, 122 (2014)
78. R. Teimuri-Mofrad, M. Gholamhosseini-Nazari, E. Payami, S. Esmati, Res. Chem. Intermed. **43**, 7105 (2017)

Affiliations

Sakineh Mozaffarnia^{1,2} · Reza Teimuri-Mofrad¹  · Mohammad-Reza Rashidi²

¹ Department of Organic and Biochemistry, Faculty of Chemistry, University of Tabriz, Tabriz 51664, Iran

² Research Center for Pharmaceutical Nanotechnology, Tabriz University of Medical Sciences, Tabriz, Iran